INTERNATIONAL UNION OF PURE AND APPLIED CHEMISTRY

ANALYTICAL CHEMISTRY DIVISION
COMMISSION ON MICROCHEMICAL TECHNIQUES AND TRACE ANALYSIS*

DISTRIBUTION ANALYSIS OF MAJOR AND TRACE ELEMENTS THROUGH SEMICONDUCTOR LAYERS OF CHANGING MATRIX USING SECONDARY ION MASS SPECTROMETRY (SIMS)†

Prepared for publication by
A. A. GALUSKA[1] and G. H. MORRISON[2]

[1]Materials Sciences Laboratory, The Aerospace Corporation,
El Segundo, California 90245, USA
[2]Department of Chemistry, Cornell University,
Ithaca, New York 14853, USA

†Series title: General Aspects of Trace Analytical Methods: Part VIII

Distribution analysis of major and trace elements through semiconductor layers of changing matrix using secondary ion mass spectrometry (SIMS)

Abstract – Secondary ion mass spectrometry is often used to monitor ele-
mental distributions in solids and at solid interfaces. The technique is
highly sensitive for most elements and has good depth resolution. How-
ever, the complexity of the sputtering event has made quantitative analy-
sis difficult, especially in multimatrix samples where changing matrix
effects are encountered. Due to the increasing importance of multilayer-
multimatrix samples in semiconductor device technology, matrix effect
calibration for quantitative SIMS analyses in these samples is essen-
tial. In this article, the current status of quantitative SIMS analysis
in layered multimatrix samples is presented. First, the basics of SIMS
quantification and theories describing matrix effects will be reviewed.
Matrix effect calibration and depth profile corrections for $Al_xGa_{1-x}As$
multilayers will then be examined. Next, a method of extending these
calibrations to the remaining IIIA-VA semiconductors will be presented.
Finally, future trends in matrix effect calibration and depth profile
correction will be discussed.

1. INTRODUCTION

In the past, semiconductor technology was largely limited to silicon technology.
Electronic devices were rather large and simple in construction. Current trends
in semiconductor technology involve the fabrication of smaller ($\leq$ 2.0 µm) and more
complex electronic structures composed of an increasing variety of materials. In
particular, microwave and optoelectronic devices composed of group IIIA – VA and
IIB – VIIA compound semiconductors are being rapidly developed using growth tech-
niques such as molecular beam epitaxy (MBE) and metal-organic chemical vapor depo-
sition (MOCVD). An increasing number of these compound semiconductor devices are
making use of superlattice structures, alternating thin lattice-matched semicon-
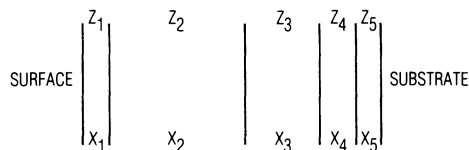ductor layers of varying composition (Fig. 1).

Fig. 1. A hypothetical $Al_xGa_{1-x}As$ super-
lattice. The thickness Z of the layers
can vary from several nanometers to
several micrometers while x can be
varied from 0 to 1 (ref. 38).

There is a tremendous need for major and trace element quantification through
these semiconductor structures. There are a few surface analysis techniques, such
as Rutherford backscattering spectrometry (RBS) and Auger electron spectrometry
(AES), which have the necessary depth resolution ($\leq$ 10 nm) and sensitivity to
examine the distribution of the major elements. However, secondary ion mass spec-
trometry (SIMS) is the only technique capable of simultaneously measuring major
and also trace (~ 1 µg/g) elemental depth distributions. Consequently, SIMS has
great potential for the characterization of these semiconductor structures.

Due to the complexity of the sputtering and ion emission processes, quantitative
SIMS analyses are difficult to obtain. As a result, the full potential of SIMS
has not been realized. Every measurement is influenced by the uncertainty due to
statistical fluctuations in the measured secondary ion current and systematic
uncertainties related to experimental conditions as well as sample character-
istics. For trace elements in homogeneous matrices, these sources of error can
generally be eliminated or reduced to the point that quantitative measure-
ments (~ 15% relative standard deviation) can be made. Conversely, quantitative

analysis in heterogeneous matrices has been severely limited due to the uncharacterized variation of secondary ion yields and sputtering yields with sample matrix (matrix effects). A depth profile of a sample composed of more than one matrix (in particular layers of different matrices stacked one on top of the other) becomes distorted by the variation of secondary ion yields and sputtering yields with matrix: signal and time are no longer proportional to concentration and depth, respectively.

Despite these difficulties, the proper calibration of ion yields and sputtering yields with matrix can make quantitative SIMS depth profiling possible for these multilayer - multimatrix samples. In this article, procedures for quantifying SIMS depth profiles through layers of IIIA - VA semiconductors will be described. First, the basics of SIMS quantification and theories describing matrix effects will be reviewed. Matrix effect calibrations and depth profile corrections for $Al_xGa_{1-x}As$ multilayers will then be examined. Next, a method of extending these calibrations to the remaining IIIA - VA semiconductors will be presented. Finally, future trends in matrix effect calibration and depth profile correction will be discussed.

2. SIMS QUANTIFICATION

When a solid surface is bombarded by energetic (5-20 keV) primary ions, the elements present are sputtered primarily as neutrals, although positive ions, negative ions, and polyatomic ions are also formed. Typically, only the secondary ion intensities of the monomeric ions, either M^+ or M^-, are used in SIMS elemental quantification. The relationship between the number of analyte ions detected I_M (counts) and the isotopically corrected analyte concentration C_M (atoms-m^{-3}) in the sample surface can be defined as

$$I_M = \tau_M C_M S_M J A_o T N^{-1} \tag{1}$$

where τ_M, S, J, and A_o are the useful ion yield, sputtering yield, ion current density (ions-m^{-2}-s^{-1}), and analysis area (m^2), respectively. T is the analysis time (s), and N is the atomic density (atoms-m^{-3}) of the sample matrix. The useful ion yield is defined as the ratio of the number of analyte ions, $M^{\pm}$, detected to the number of analyte atoms sputtered from the specimen. Useful ion yields are also defined as the product of the probability of $M^{\pm}$ formation ($\beta^{\pm}$) and the transmission efficiency (η). The sputtering yield is defined as the average number of atoms sputtered by each incident primary ion. It is assumed that the elemental components of the sputtering yield are proportional to the bulk elemental concentrations.

The difficulty in solving Eq. 1 for analyte concentration is that useful ion yields and sputtering yields are influenced by a variety of factors, and can vary drastically from sample to sample. Useful ion yields can vary by orders of magnitude for different elements in the same matrix, and for the same element in different matrices (ref. 1-4). In addition, useful positive ion yields are increased by the presence of electronegative elements such as oxygen (ref. 5), and useful negative ion yields are increased by the presence of electropositive elements such as cesium (ref. 6). Sputtering yields are also different for different elements in the same or different sample matrices. Sputtering yields are influenced by the following: the masses of incident and target atoms, primary ion energy and current density, sample lattice crystallinity and orientation, surface-binding energy, and the angle of incidence between the primary ion beam and the sample surface (ref. 7-9). Consequently, useful ion yields and sputtering yields must be determined for each and every element and sample matrix. In addition, due to the fluctuating experimental conditions with time, these values must be determined each time quantification is performed in the same sample matrix.

For pure elemental matrices, sputtering yields can be determined experimentally from the sputtering rate $\overset{\circ}{Z}$ (m-s^{-1}). After sputtering, the depth of the sputtered crater is measured using a profilometer or an optical interferometer. Dividing this depth by the sputtering time interval yields the average sputtering rate. If one makes the approximation that the crater walls behave as step functions, the sputtering yield may be determined from

$$S = \overset{\circ}{Z}ANi_p^{-1} \tag{2}$$

where A is the crater area (m^2), and i_p is the primary beam current (ions-s^{-1}).

In matrices of more than one element, differences in elemental sputtering yields (preferential sputtering) result in composition changes in the near surface region

(ref. 10, 11). Elements which sputter slowly are enriched at the surface while elements which sputter rapidly are depleted from the surface. These compositional changes usually occur over a short depth increment (approximately twice the range of the primary ion) after which a steady state condition is reached. At this point, the elemental components of the sputtering yield are proportional to the bulk elemental concentrations. Once this steady state condition has been reached, Eq. 2 can be incorporated into Eq. 1 to obtain a more useful form of the ion intensity equation.

$$I_M = \tau_M C_M^o \bar{z} A_o T \tag{3}$$

Equations 1 and 3 can now be solved for the analyte concentration providing τ_M can be accurately determined. Useful ion yields can be approximated using semitheoretical techniques (ref. 12-16), but they are most accurately determined using homogeneous bulk standards or ion implanted standards (ref. 17-20) fabricated from the same matrix as the unknown sample.

While useful ion yields can be determined from standards, they can change quite dramatically between analyses. Secondary ion collection and instrumental transmission are influenced by operator adjustment and indeterminate instrumental fluctuations which occur during routine operation. To reduce this effect, it is common practice to use relative sensitivity factors (RSF), as given by Eq. 4, in which the τ of an analyte is ratioed to that of a reference element of known concentration in the sample matrix.

$$\begin{aligned} RSF &= \tau_a \tau_{ref}^{-1} \\ &= (I_a C_{ref})(I_{ref} C_a)^{-1} \end{aligned} \tag{4}$$

The normalization procedure is designed to minimize the influence of instrumental variations.

3. MATRIX EFFECTS

The fabrication of external and internal standards by ion implantation has provided an accurate (15% relative standard deviation) means of quantifying trace element distributions in homogeneous matrices. However, due to the uncharacterized variation of secondary ion yields and sputtering yields with matrix composition (matrix effects), the quantitative SIMS analysis of heterogeneous matrices remains a problem. To overcome this difficulty, the mechanisms underlying matrix effects must be more clearly understood. Several factors are known to influence matrix effects. These include the bulk matrix composition and the surface concentration of reactive species (electronegative elements such as oxygen or electropositive elements such as cesium), which can either be adsorbed from the sample chamber during analysis or implanted as a primary ion. Several explanations for matrix effects, which depend to varying extents on the bulk composition and the reactive species concentrations have been proposed. The sputtering yield, compositional, and oxide bond approaches to matrix effect calibration will be presented and briefly discussed.

Sputtering yield approach

The sputtering yield approach to matrix effect calibration is based on the fact that positive and negative ion yields are greatly enhanced by the incorporation of oxygen or cesium, respectively, in the sputtered surface. Deline et al. (ref. 21-23) state that for reactive beam sputtering "ion yield matrix effects arise solely from variations in the substrate sputtering yields." They justify this statement by asserting that implanted oxygen and cesium are responsible for the observed matrix effects, and that the equilibrium concentration, [R], of these reactive species is determined by the sputtering yield, S.

This relationship between [R] and S is derived from equations describing ion implantation during sputtering (ref. 24, 25):

$$[R] = \alpha N S^{-1} \tag{5}$$

$$C_s = [R]([R] - N)^{-1} = \alpha(\alpha + S)^{-1} \tag{6}$$

where α is the accommodation coefficient (which equals $1 - B$, where B is the backscattering coefficient), N is the atomic density of the sample surface, and C_s is the atomic fraction of implanted projectiles in the surface. In their declaration, Deline et al. assume that $\alpha = 1$, N and S are constant, and that there is no

preferential sputtering. In their experiments, they make the further assumption that when primary current density is constant, the sputtering rate is approximately proportional to the sputtering yield regardless of N.

The final result of these approximations is the relationship

$$\tau \propto [R] \propto (1/S)^y \propto (1/\frac{Q}{Z})^y_J = const \tag{7}$$

where y is a constant determined experimentally for each analyte. Plots of log (τ) versus log $(1/\frac{Q}{Z})$ obtained by Deline <u>et</u> <u>al</u>. (ref. 21-23) and others (ref. 26) for various elements have been roughly linear. The sputtering yield approach, however, has been severely criticized (ref. 27-30) because of the many unjustified assumptions that are made. It is likely that other matrix effects are present within the experimental error of the data (ref. 27). Various attempts to experimentally determine the relationship between [R] and S using Auger spectroscopy have both supported and contradicted the proposed relationship (ref. 23, 28-30). It is unclear when the sputtering yield approach applies or does not apply.

Compositional approach

The compositional approach is based on experiments, performed on selected ternary metal alloys and silicates which show a linear relationship between useful ion yields and matrix composition (ref. 31-33). Using oxygen flooding in conjunction with a low current density Ar^+ primary beam, the sample surfaces were saturated with oxygen. Thus, the effects of reactive species enhancement were standardized. The remaining matrix induced variations of useful ion yields were then explained using the expression

$$\tau_M = \Sigma^n_{i=1} P_{M,i} C_i \tag{8}$$

where τ_M is the useful ion yield of element M, $P_{M,i}$ is a parameter representing the influence of element i on the ion yield of element M, C_i is the mole fraction of element i.

For quantitative analysis based on this approach, relative sensitivity factors were obtained using Eq. 8 to described the useful ion yields of both the analyte and the reference. Relative sensitivity factors obtained by such a calculation were shown to agree with the experimentally determined values to an accuracy of 1 - 7% RSD for various metals in silicate glasses (ref. 33). Despite the success of this method in the cases studied, it has not been successfully applied to other types of samples. Although the reason for its limited use has not been stated in the literature, it is probably related to the difficulty of saturating many metals (such as those containing Pd, As, and Pt) and semiconductor (most IIIA-VA semiconductors) surfaces with oxygen without significantly degrading instrumental performance (ref. 28).

Oxide bond approach

The oxide bond explanation of matrix effects is based on the work of Yu and Reuter (ref. 34-35). They performed SIMS analyses on various binary metal alloys under both O_2^+ bombardment and Ar^+ bombardment with oxygen flooding. After the SIMS analyses, the alloys were then analyzed with X-ray photoelectron spectroscopy (XPS) to determine the types of metal oxides formed and the extent of oxidation.

The XPS data from the pure elemental metals showed that oxidation was more extensive for those metals which form metal oxides with large negative Gibbs energies of formation than those metals which form oxides with less favorable Gibbs energies of formation. The addition of the second alloy component resulted in significant changes in oxidation, ionization probability, and ion energy distribution for both components. The observed trends can be summarized by two general rules. First of all, for an alloy A-B, where A forms a stronger oxide bond than B, the presence of A enhances the oxidation and also the ion yield of B, while the presence of B suppresses the oxidation and also the ion yield of A. Secondly, the presence of A sharpens the energy distribution of B^+, while the presence of B broadens the energy distribution of A^+. Both the trends in ion yield and ion energy distribution were attributed to the relative extent of surface oxidation.

The influence of surface oxidation has been attributed both to changes in the work function of the surface and also to changes in the bond breaking mechanism of the surface (ref. 36). While these rules were firmly supported by data, they were never applied to any type of matrix effect calibration for quantitative SIMS analysis.

4. MATRIX EFFECT CALIBRATION FOR $Al_xGa_{1-x}As$ MATRICES

There have been only a few investigations of the influence of matrix effects on the ion yields and sputtering yields of IIIA - VA semiconductors. For homologous series of compounds, such as $Al_xGa_{1-x}As$ and $GaAs_xP_{1-x}$ matrices, under both O_2^+ and Cs^+ bombardment, Katz (ref. 37) observed that sputtering yields were linearly related to the changing matrix composition. Similarly, for $Al_xGa_{1-x}As$ matrices under O_2^+ bombardment, others (ref. 30, 38) have observed that the practical ion yields of major and trace elements were linearly related to the matrix composition defined by x. While these investigations showed that linear relationships existed, precise and reproducible matrix effect calibration lines could not be obtained due to the indeterminate variation of instrumental parameters which alter the observed ion yields and sputtering yields between analyses. A method of normalizing out these instrumental parameters was required.

The significance of instrumental variations and procedures for normalizing out their influence were examined by Galuska and Morrison (ref. 38). Using an O_2^+ primary ion beam, they performed a series of analyses on groups of ion implanted $Al_xGa_{1-x}As$ matrices. To ensure near identical analysis conditions during each analysis period, groups of samples, including in each case GaAs, were inserted simultaneously. These samples were sequentially analyzed without manipulating any instrumental parameters. While minimizing instrumental variations in this way, the useful ion yields (τ) of the trace and major elements were obtained. These useful ion yields were then ratioed to produce relative sensitivity factors (RSF) and relative ion yields ($R\tau$).

$$R\tau = \tau_x\tau_o^{-1} \qquad\qquad (9)$$

τ_x is the useful ion yield of the analyte in a particular $Al_xGa_{1-x}As$ matrix, and τ_o is the useful ion yield of the analyte in GaAs when both measurements are performed under nearly identical conditions.

The linearity, precision, and reproducibility of matrix effect calibration lines formed using τ's, RSF's and $R\tau$'s were then compared. The results for Be, Si, P, B and As are presented in Tables 1, 2 and 3. The calibration lines obtained using relative ion yields were the most linear, precise, and reproducible. As expected,

TABLE 1. Useful ion yield calibrations for $Al_xGa_{1-x}As$ matrices (ref. 38).

Analyte	Week No.	X Values	Intercept ($\times 10^{-7}$)	Linear Slope ($\times 10^{-5}$)	RSD Correlation (r^2)	RSD Slope (%)
^9Be	1	0,0.12,0.26,0.37	1.23	41.5	0.927	32.8
	2	0,0.13,0.21,0.37	116	67.3	0.915	68.6
	3	0,0.13,0.18,0.21	61.4	32.3	0.995	9.5
^{28}Si	1		36.4	22.2	0.989	18.5
	2		25.3	15.2	0.987	17.0
	3		38.9	17.7	0.984	10.8
^{31}P	16	0,0.18,0.26,0.31	0.822	0.291	0.936	18.6
	32	0,0.13,0.18,0.37	1.17	0.258	1.000	2.0
^{11}B	16		25.8	7.05	0.734	53.6
	32		28.2	17.0	0.994	8.7
^{75}As	1		1.78	0.130	0.966	14.6
	2		0.932	0.0891	0.915	21.0
	3		0.940	0.108	0.984	11.0
	32		0.918	0.0532	0.932	11.2
		Av RSD per Point = 18.4%				
^9Be	total		31.4	44.7	0.868	12.3
^{28}Si	total		11.0	19.0	0.994	5.8
^{31}P	total		1.00	0.278	0.928	12.4
^{11}B	total		27.0	15.3	0.825	18.8
^{75}As	total		0.642	0.111	0.722	19.2
		Av RSD per Point = 60.4%				

TABLE 2. Relative sensitivity factor calibrations for $Al_xGa_{1-x}As$ matrices (ref. 38).

Analyte	Week No.	X Values	Intercept ($\times 10^{-7}$)	Slope ($\times 10^{-5}$)	Linear Correlation (r^2)	RSD Slope (%)
$^9Be/^{75}As$	1	0,0.12,0.26,0.37	47.0	890	0.731	33.6
	2	0,0.13,0.21,0.37	84.8	573	0.894	23.0
	3	0,0.13,0.18,0.21	66.5	950	0.995	4.7
$^{28}Si/^{75}As$	1		39.8	271	0.708	38.2
	2		39.4	382	0.903	24.2
	3		36.0	711	0.936	37.8
$^{31}P/^{75}As$	16	0,0.18,0.26,0.31	1.58	9.67	0.715	40.3
	32	0,0.13,0.18,0.37	1.88	4.91	0.827	58.9
$^{11}B/^{75}As$	16		30.7	454	0.945	26.1
	32		60.9	509	0.940	17.1

Av RSD per Point = 10.4%

Analyte	Week No.	X Values	Intercept ($\times 10^{-7}$)	Slope ($\times 10^{-5}$)	Linear Correlation (r^2)	RSD Slope (%)
$^9Be/^{75}As$	total		88.7	740	0.694	16.8
$^{28}Si/^{75}As$	total		42.7	357	0.804	17.7
$^{31}P/^{75}As$	total		2.41	4.45	0.464	79.2
$^{11}B/^{75}As$	total		34.0	481	0.883	19.2

Av RSD per Point = 24.4%

TABLE 3. Relative ion yield calibrations for $Al_xGa_{1-x}As$ matrices (ref. 38).

Analyte	Week No.	X Values	Intercept ($\times 10^{-7}$)	Slope ($\times 10^{-5}$)	Linear Correlation (r^2)	RSD Slope (%)
^9Be	1	0,0.12,0.26,0.37	1.0	52.9	0.999	6.4
	2	0,0.13,0.21,0.37	1.0	42.6	0.996	4.3
	3	0,0.13,0.18,0.21	1.0	41.7	1.000	14.2
^{28}Si	1		1.0	44.5	1.000	9.8
	2		1.0	40.1	0.975	5.7
	3		1.0	45.9	1.000	9.6
^{31}P	16	0,0.18,0.26,0.31	1.0	21.2	0.995	9.6
	32	0,0.13,0.18,0.37	1.0	23.0	1.000	2.5
^{11}B	16		1.0	46.7	0.990	10.7
	32		1.0	39.5	1.000	8.6
^{75}As	1		1.0	6.00	0.933	15.7
	2		1.0	6.54	0.991	2.8
	3		1.0	5.76	0.980	12.4
	32		1.0	5.32	0.925	11.0

Av RSD per Point = 7.4%

Analyte	Week No.	X Values	Intercept ($\times 10^{-7}$)	Slope ($\times 10^{-5}$)	Linear Correlation (r^2)	RSD Slope (%)
^9Be	total		1.0	46.3	0.981	13.7
^{28}Si	total		1.0	44.7	0.986	5.0
^{31}P	total		1.0	22.1	0.942	4.6
^{11}B	total		1.0	46.6	0.961	7.0
^{75}As	total		1.0	5.76	0.917	7.0

Av RSD per Point = 9.2%

TABLE 4. Relative sputtering yield calibrations for $Al_xGa_{1-x}As$ matrices

Week No.	Intercept	Slope	Linear Correlation (r^2)	RSD Slope (%)
1	1.0	-1.00	0.928	11.8
2	1.0	-1.01	0.913	12.5
3	1.0	-0.89	0.991	4.0
16	1.0	-0.89	0.997	3.2
32	1.0	-0.75	0.934	11.6
		Av RSD per Point = 3.8%		
total	1.0	-0.86	0.906	8.3
		Av RSD per Point = 7.9%		

the calibration lines obtained using useful ion yields were linear, but exhibited poor precision and reproducibility. Despite good reproducibility (~ 24.4%) for a given data point, the relative sensitivity factors produced calibration lines with poor linearity, precision, and reproducibility. The superiority of $R\tau$'s over RSF's for matrix effect calibration is readily justified. An $R\tau$ is directly proportional to the ion yield of the analyte while an RSF is related to the ion yields of both the analyte and the reference. Since the influence of instrumental variations on the ion yields of the analyte and reference can vary independently, RSF's are altered by instrumental changes to a greater extent than $R\tau$'s. Moreover, $R\tau$'s are designed to normalize matrix effects to a standard matrix while RSF's are not.

In addition to τ's, RSF's and $R\tau$'s, absolute sputtering yields and relative sputtering yields (RS) were also determined as a function of matrix composition. As shown in Table 4, the calibration lines obtained using relative sputtering yields (where $RS = S_x S_o^{-1}$) were quite precise and reproducible. The absolute sputtering yields were not. The use of $R\tau$'s and RS's has allowed the influence of matrix changes on ion yields and sputtering yields to be precisely calibrated (~ 10% RSD) for the first time.

5. QUANTITATIVE ANALYSIS OF $Al_xGa_{1-x}As$ MULTILAYERS

Through the use of $R\tau$ and RS calibration lines, the quantitative SIMS analysis of $Al_xGa_{1-x}As$ multilayers (superlattices) has become possible. The only requirement is that a GaAs standard be analyzed under the same conditions as the sample of interest. The concentration of analyte at each point of a depth profile C_p (atom-m^{-3}) can be determined using Eq. 10.

$$C_p = I_p (R\tau_x \tau_o z_p A_o)^{-1}$$ (10)

$R\tau_x$ is the relative ion yield determined from a calibration line for the appropriate value of x, and τ_o is the useful ion yield of the analyte in the standard matrix (GaAs). I_p is the signal and z_p is the depth increment associated with each point of the depth profile. Similarly, the erosion rate at each point of a depth profile $\overset{o}{z}_p$ can be determined using Eq. 11.

$$\overset{o}{z}_p = RS_x \overset{o}{z}_o N_o N_x^{-1}$$ (11)

RS_x is the relative sputtering yield determined from a calibration line for the appropriate value of x, and $\overset{o}{z}_o$ is the sputtering rate of the standard matrix (GaAs). N_o and N_x are the atomic densities of the standard matrix and the sample, respectively.

The application of Eqs. 10 and 11 requires a knowledge of the matrix composition (x) at each data point. While this information is not readily available from an uncalibrated SIMS depth profile, a program, SLIC-superlattice and interface calibration (ref. 39) has been developed which determines x at each data point using the $^{75}As^+$ calibration line, the RS calibration line, and the fact that the As concentration is constant in $Al_xGa_{1-x}As$ matrices. If the value of $R\tau_x$ in Eq. 10 is expressed in terms of the equation for the $^{75}As^+$ calibration line ($R\tau_{As,x} = xM_{As,R\tau} + 1$; where $M_{As,R\tau}$ is the slope of the line), the equation can be manipulated to the following form:

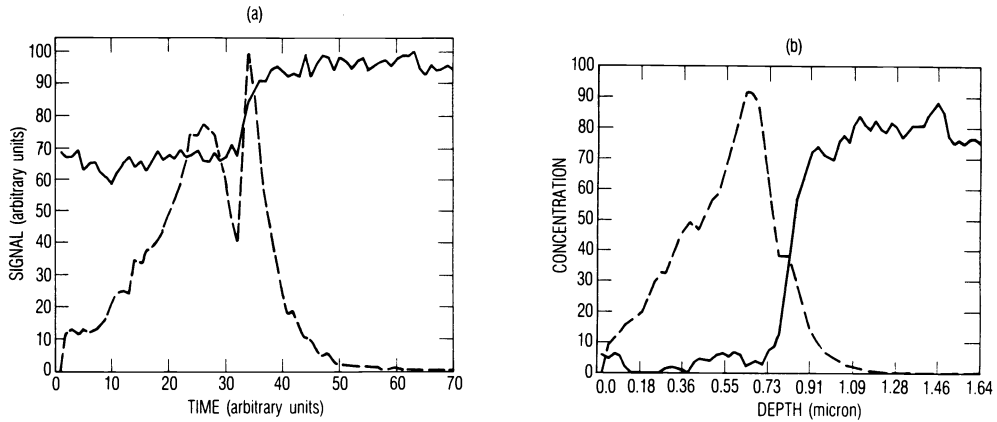$$x = \{ I_{As,p} (C_{As,p} A_o \tau_{As,o} z_p)^{-1} - 1 \} M_{As,R\tau}^{-1}$$ (12)

Fig. 2.   SIMS depth profile of a 250 keV $^{11}B^+$ implant into a GaAs/Al$_{0.12}$Ga$_{0.88}$As/GaAs sample: (a) uncorrected profiles of $^{11}B^+$ (---) and $^{75}As^+$ (——), (b) concentration profiles of B(---) [2.0×10^{24} atoms-m^{-3} fullscale] and Al (——) [1.0×10^{28} atoms-m^{-3} full scale] (ref. 38).

Except for z_p, the values for all the variables on the right side of Eq. 12 can be readily determined.   Since z_p is directly related to $\overset{o}{z}$ ($z_p = \overset{o}{z} \, T_p$; where T_p is the number of seconds per point), it can be expressed in terms of Eq. 11.   If RS_x is replaced with the corresponding equation for the RS calibration line, Eq. 13 is obtained

$$z_p = (M_{RS} \, x + 1) \, \overset{o}{z}_o \, N_o N_x^{-1} T_p$$

$$= (M_{R\overset{o}{z}} \, x + 1) \, \overset{o}{z}_o \, T_p \qquad\qquad (13)$$

M_{RS} is the slope of the RS calibration line, and $M_{R\overset{o}{z}}$ is the slope of the corresponding relative erosion rate calibration line ($M_{R\overset{o}{z}} = M_{RS}N_x N_o^{-1}$).   Once again the values of z_p and x are the only unknown quantities.

SLIC initially assumes that the x = 0.   The corresponding value of z_p is then determined from Eq. 13 and employed in Eq. 12 to obtain a better approximation of x.   This process is iterated until the values of x and z_p converge.   In this manner, the matrix composition and depth at each point of a depth profile are determined through matrix gradients, interfaces and plateaus.   The dopant profiles are then corrected for matrix changes at each data point using Eq. 10, and the appropriate dopant calibration lines.

A 250 keV $^{11}B^+$ implant into a layered sample (GaAs/Al$_{.12}$Ga$_{.88}$As/GaAs) provides a good example for the correction of matrix effects.   In Fig. 2a, the uncorrected SIMS depth profile of $^{11}B^+$ and $^{75}As^+$ in this sample is presented.   The first interface occurs at 33 time units while the second interface has not been reached in this profile.   Due to matrix effects, the vertical and horizontal scales are no longer linearly related to concentration and depth, respectively.   The peak in the $^{11}B^+$ profile at 34 time units is a good example of a distortion introduced by the changing matrix effects at the interface.   In Fig. 2b, the horizontal scale has been transformed into depth, and the concentration of Al at each point has been calculated from the $^{75}As^+$ profile.   The $^{11}B^+$ profile was then quantified.   An Al concentration of 2.4×10^{27} atom-m^{-3} ± 6.0% was calculated for the Al$_x$Ga$_{1-x}$As layer which agrees quite well with the value expected from MBE growth parameters.   The correction procedure has also removed the distorted interface region of the $^{11}B^+$ profile, transforming the profile into the slightly distorted Gaussian shape, which was expected.

The most crucial factor influencing the quality of the matrix corrections performed by SLIC is the accuracy with which the matrix structure can be determined.   This accuracy has been checked with RBS.   RBS analysis is accurate to about 10% RSD, and has a detection limit of 1% for Al$_x$Ga$_{1-x}$As matrices.   In Fig. 3, a complex Al$_x$Ga$_{1-x}$As sample was analyzed by SIMS and RBS, respectively. The Al concentration at specific regions of the superlattice was determined using SLIC and standard RBS techniques (ref. 40).   As shown in Table 5, the values determined by the two techniques agree quite well.   In fact, the two sets of data are not statistically different at a 95% confidence level.
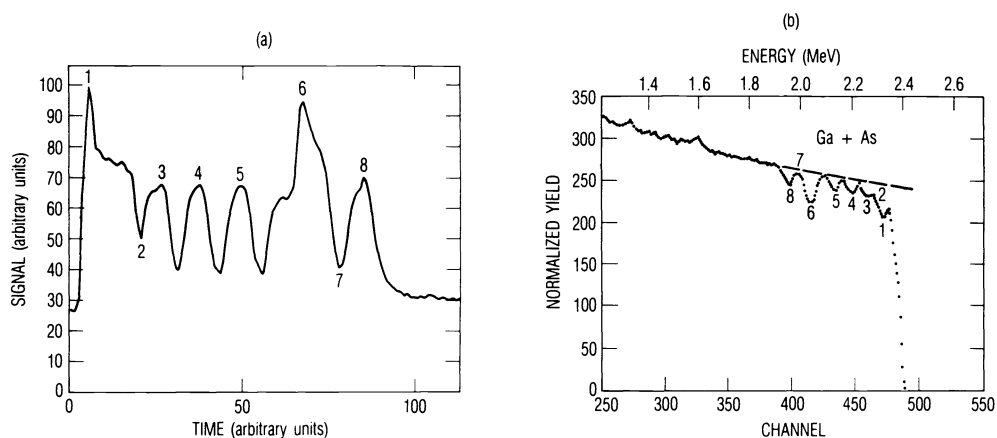
Fig. 3. SIMS and RBS depth profiles of an $Al_xGa_{1-x}As$ superlattice: (a) an uncor-
rected $^{75}As^+$ SIMS profile; (b) an RBS profile of the total counts from Ga and As
(ref. 38).

TABLE 5. Point-by-point comparison of Al concentrations determined by
SIMS and RBS analyses (ref. 39).

Al Concentration (X 10^{27} atom-m^{-3})

Point	RBS	SIMS	Deviation
1	12.0	13.0	-1.0
2	4.2	3.9	+0.3
3	5.1	4.8	+0.3
4	5.1	4.7	+0.4
5	5.2	4.7	+0.5
6	11.0	11.0	0.0
7	1.0	1.3	-0.3
	4.9	5.7	-0.8

AVG of Deviations = -0.075

In addition to matrix composition, the point-by-point correlation between matrix
structure and dopant distribution is critical.   Small differences between the
actual and the measured matrix structure can significantly influence the correc-
tions performed on dopant distributions.   As apparent in Fig. 4, the $^{75}As^+$ signal
tracks the Al distribution quite well.   SLIC uses this correlation to precisely
determine matrix structures.   However, errors can still result from the correla-
tion between matrix structure and dopant distribution.   For example, there is a
dead time between the measurement of the matrix signal and the dopant signal for
each point of a depth profile.   When this dead time is large compared to the
abruptness of the matrix changes, the matrix and dopant signals will be obtained
from different matrix regions.   Consequently, the dopant signal will be calibrated
for the wrong matrix composition.   Such an error is shown in Fig. 5.   Fortunately,
this type of error can usually be avoided by minimizing the dead time and reducing
the sputtering rate.

The full utility of SLIC can be appreciated when very complex samples are
analyzed.   An uncorrected SIMS depth profile of a complex $Al_xGa_{1-x}As$ superlattice
grown by MBE with Be and Si dopants is presented in Fig. 6a.   In Fig. 6b, SLIC has
been used to quantify the elemental distributions in this sample.   In the uncor-
rected profile both the Be and Si distributions follow the $^{75}As^+$ signal due to the
changing matrix effects.   Upon calibration, both the Be and Si distributions have
changed substantially.   As expected from the MBE growth conditions, the Be concen-
tration generally increases as the Al concentration decreases and vice versa.   In
addition, excluding the surface buildup, the Si distribution has generally leveled
out at 4 x 10^{24} atom/m^3.   Without SLIC, this type of analysis could not have been
made.   At the present, SLIC represents the only successful attempt at using SIMS
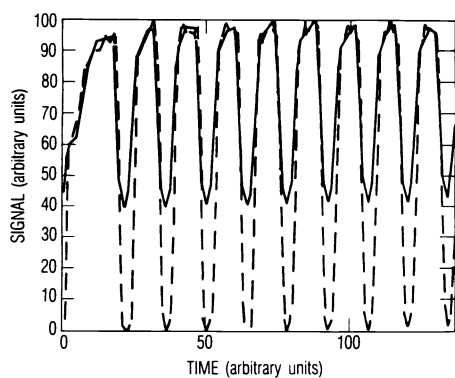to quantify elemental distributions through multilayers of changing matrix.

Fig. 4. An uncorrected SIMS depth profile of $^{75}As^+$ (———) and $^{27}Al^{2+}$ (---) in an $Al_xGa_{1-x}As$ superlattice (ref. 38).

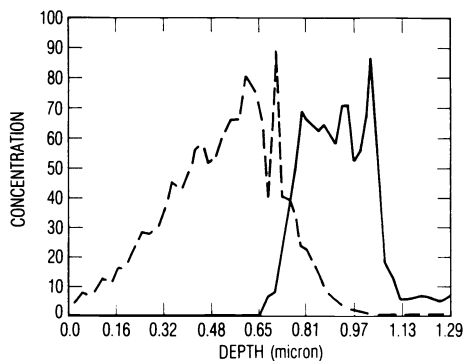Fig. 5. A matrix corrected SIMS depth profile of a 250 keV $^{11}B^+$ implant into a $GaAs/Al_{0.30}Ga_{0.70}As$ sample with a matrix-dopant mismatch at the interface located at a depth of approximately 0.69 μm (B conc. (...) [2 x 10^{24} atoms-m^{-3} full scale] and Al conc. (———) [1 x 10^{28} atoms-m^{-3} full scale]) (ref. 39).
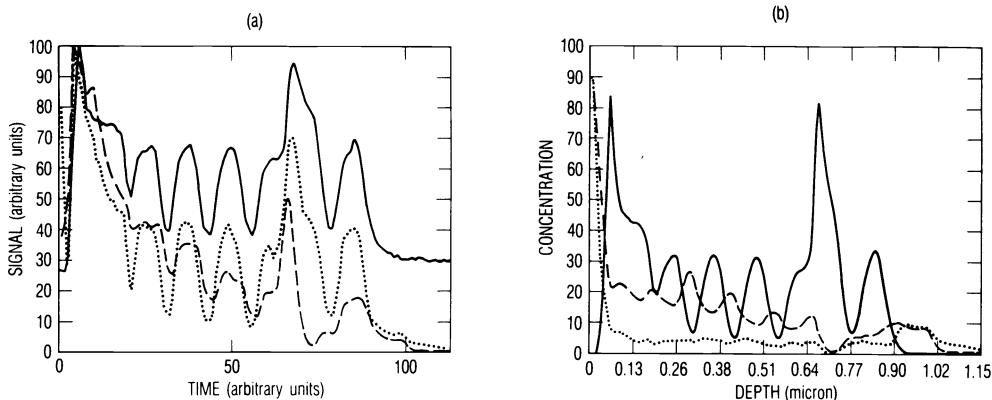
(a)

(b)

Fig. 6. SIMS depth profile of a $Al_xGa_{1-x}As$ superlattice doped with Be and Si: (a) uncorrected profiles of $^9Be^+$ (---), $^{28}Si^+$ (...), and $^{75}As^+$ (———); (b) concentration profiles of Be (---) [5.0 x 10^{25} atoms-m^{-3} full scale], Si (...) [9.0 x 10^{25} atoms-m^{-3} full scale], and Al (———) [1.5 x 10^{28} atom-m^{-3} full scale] (ref. 39).

6. EXTENDED MATRIX EFFECT CALIBRATION

While the initial attempts at matrix effect calibration and correction have been successful for $Al_xGa_{1-x}As$ matrices, the general application of such calibration procedures to a greater variety of matrices requires a better understanding of the fundamental processes involved. During their attempts to extend the $Al_xGa_{1-x}As$ matrix effect calibration lines to other IIIA - VA semiconductors ($Ga_{0.47}In_{0.53}As$, GaSb, InSb, InP, GaP, and $Al_xGa_{1-x}As$ matrices were analyzed.), Galuska and Morrison (ref. 41) examined the applicability of the sputtering yield, compositional, and oxide bond explanations of matrix effects. As before, the analyses were performed using an O_2^+ primary ion beam. To reduce experimental errors, practical ion yields and sputtering yields were replaced with RT and RS, respectively.

The sputtering yield hypothesis was evaluated directly using Eq. 7. The compositional approach was examined in conjunction with the oxide bond approach. The parameter $P_{M,i}$ from Eq. 8 was treated as a measure of the affinity of element i for oxygen. The values of $P_{M,i}$ were approximated from the average bond energies of the diatomic metal oxides.

According to the compositional theory, plots of RT versus the average matrix-oxygen bond energy should yield straight lines. Similarly, according to the sput-
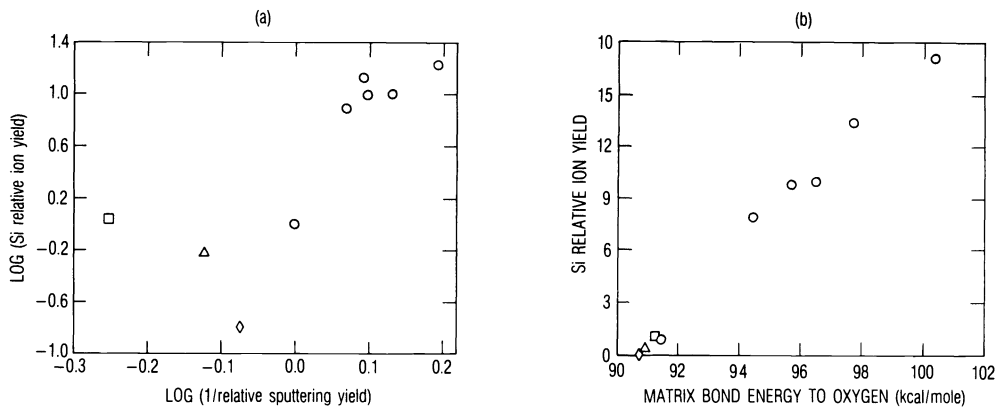
Fig. 7. Influence of matrix effects on the τ value of ^{28}Si: (a) sputtering yield
approach; (b) compositional approach [Al$_x$Ga$_{1-x}$As-O, InP-Δ, GaSb- $\lozenge$, GaP- $\square$]
(ref. 41).

TABLE 6. Linearity of the sputtering yield and compositional approaches
to matrix calibration for group IIIA-VA compound matrices under O_2^+
bombardment (ref. 41).

LOG ($R\tau$) Versus Log (1/RS)			$R\tau$ VERSUS MATRIX OXYGEN BOND ENERGY		
Analyte	Linear Correlation (r^2)	RSD Slope (%)	Analyte	Linear Correlation (r^2)	RSD Slope (%)
^{28}Si$^+$	0.633	64.9	^{28}Si$^+$	0.999	0.28
^{9}Be$^+$	0.713	54.1	^{9}Be$^+$	0.998	0.42
^{31}P$^+$	0.731	30.8	^{31}P$^+$	0.991	0.24
^{24}Mg$^+$	0.748	21.1	^{24}Mg	0.993	0.60
^{11}B$^+$	0.534	32.9	^{11}B$^+$	0.998	0.24
^{121}Sb$^+$	0.791	16.5	^{121}Sb$^+$	0.995	0.29

tering yield hypothesis, plots of log ($R\tau$) versus log (1/RS) (RS and R$\dot{z}$ are
approximately equal for these samples.) should also yield straight lines.   The
experimental data for ^{28}Si$^+$, plotted using the two different approaches, is pre-
sented in Fig. 7a and 7b.   As apparent in these figures, the compositional theory
satisfies the linearity criteria much better than the sputtering yield approach.
The poor linearity of the sputtering yield approach is not significantly altered
by replacing RS with R$\dot{z}$. The superior linearity of the compositional approach is
emphasized in Table 6 where the linear correlations and standard deviations of the
lines for several different elements are compared.   In each case, excellent
linearity and precision were observed when using the compositional approach and
poor linearity and precision were observed when using the sputtering yield
approach.   This linearity persisted whether the analyses were performed under
O_2^+ bombardment or Ar$^+$ bombardment with oxygen flooding.   From these experiments,
it appears that the affinity of a matrix for oxygen is the critical factor (at
least for IIIA - VA semiconductors under O_2^+ bombardment) determining the variation
of ion yields with matrix.   This oxygen affinity is determined by the matrix com-
position.   While the sputtering yield does influence the amount of oxygen avail-
able for bonding, it does not determine the final oxygen content of the surface
(ref. 30).

To determine a general mechanism for matrix effects, it is important to understand
how matrix effects influence the τ's of one particular element versus another.
One can gain an insight into this phenomenon by comparing the slopes of the cali-
bration lines to the first ionization potentials of the respective analytes.   Such
a comparison is presented in Table 7.   For those elements which fall in the same
column of the periodic table [B, Al, Ga), (P, As, Sb), and (Be and Mg)], a general
relationship is observed.   Elements with larger first ionization potentials (lower
ionization probabilities) yield calibration lines of steeper slope than those with

TABLE 7. Dependence of R_T versus bond energy line slopes on first
ionization potential (ref. 41).

Analyte	Slope	Intercept	1st Ionization Potential (eV)
$^{11}B^+$	1.90	-173	8.30
$^{27}Al^+$	0.19	-17	5.98
$^{69}Ga^+$	0.25	-22	6.00
$^{31}P^+$	0.93	-84	11.02
$^{75}As^+$	0.30	-26	9.81
$^{121}Sb^+$	0.30	-26	8.64
$^{9}Be^+$	1.86	-169	9.32
$^{24}Mg^+$	0.52	-47	7.64
$^{28}Si^+$	1.88	-170	8.15
$^{7}Li^+$	0.10	-9	5.39

lower first ionization potentials (higher ionization probabilities). This indi-
cates that elements which have small ionization probabilities are influenced by
matrix effects (the amount of bound oxygen) to a greater extent than those which
have large ionization probabilities. As one might expect, this relationship is
very similar to that commonly observed for elemental τ's in a single matrix
enhanced by oxygen bombardment or flooding: the τ's of elements with small ioni-
zation probabilities are enhanced to a greater extent by the presence of oxygen
than those of elements with large ionization probabilities.

The excellent linearity of the R_T versus matrix-oxygen bond energy calibration
lines and their relationship to elemental ionization potentials can be used to
improve the quality of both qualitative and quantitative SIMS analysis. Using the
relationships expressed in these matrix calibration lines, one can anticipate when
matrix effects will be a problem, and how they may distort depth profiles of
layered multimatrix samples. For example, a largely distorted Gaussian depth
distribution would be expected for the SIMS analysis of a $^{11}B^+$ implant through a
GaAs layer into an $Al_{.30}Ga_{.70}As$ layer because $^{11}B^+$ emission is very sensitive to
the presence of oxygen, i.e., matrix effects, and $Al_{.30}Ga_{.70}As$ has a much greater
oxygen affinity than GaAs. Alternatively, a smaller distortion would be expected
for an $^{24}Mg^+$ implant and an even smaller distortion for a $^{7}Li^+$ into such a struc-
ture. The sensitivity of the τ's of these elements to matrix effects decreases
going from $^{11}B^+$ to $^{24}Mg^+$ to $^{7}Li^+$. The SIMS analyses of these implants are shown
in Fig. 8.

These calibration lines are even more valuable when a quantitative SIMS analysis
in either a single matrix or a layered multimatrix sample is desired. Since these
types of calibration lines are highly reproducible, dopant distributions in a
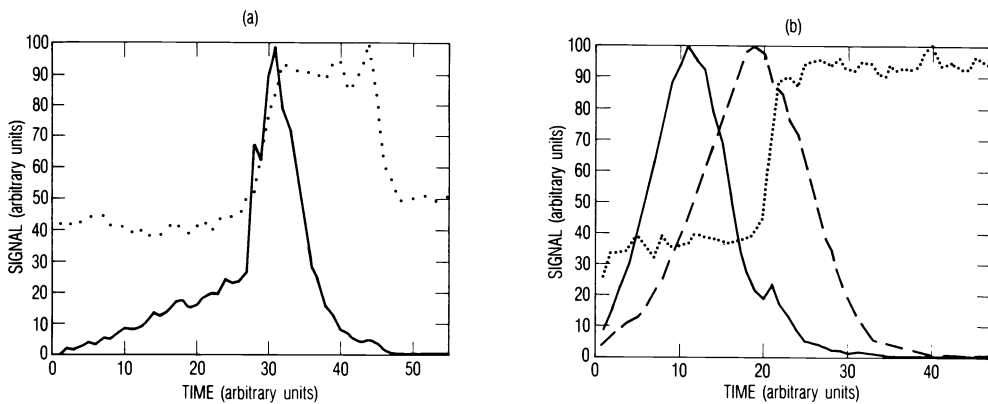

Fig. 8. SIMS analysis of $^{11}B^+$, $^{24}Mg^+$ and $^{7}Li^+$ implants through a GaAs/$Al_{0.3}$
$Ga_{0.7}As$ structure: (a) depth profiles of $^{11}B^+$ (...) and $^{75}As^+$ (——) (interface
at 31 time units); (b) depth profiles of $^{24}Mg^+$ (——), $^{7}Li^+$ (---) and $^{75}As^+$ (...)
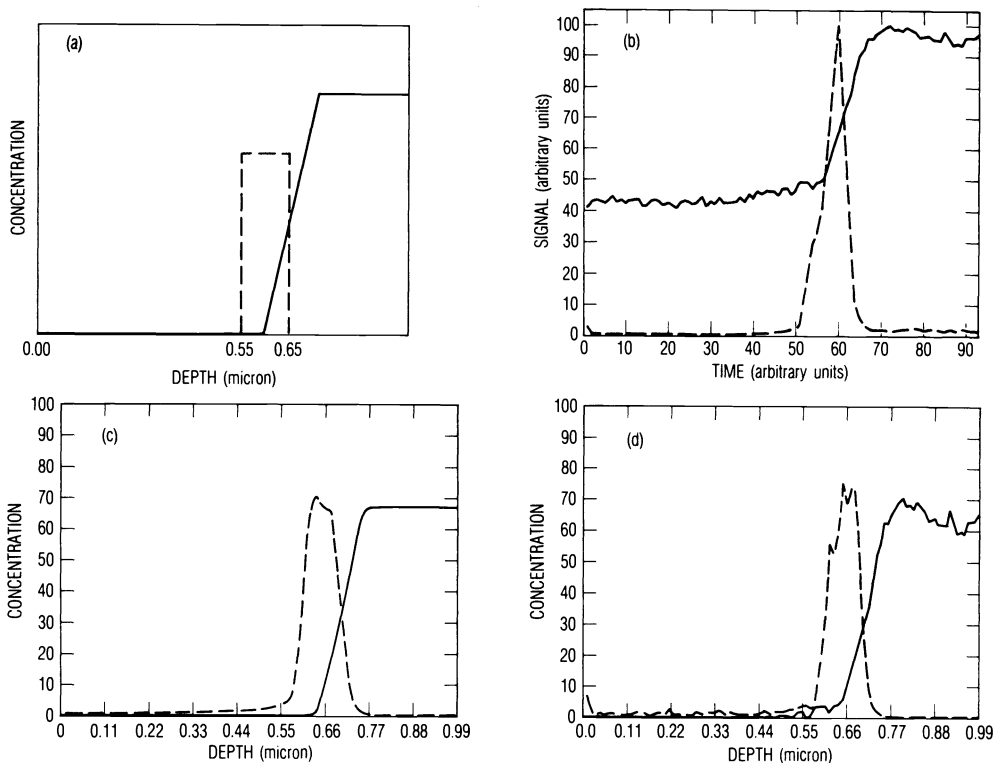(interface at 20 time units) (ref. 41).

Fig. 9. SIMS analysis of a Be plateau at a graded GaAs/Al$_{0.3}$Ga$_{0.7}$As interface: (a) hypothetical structure Be (---) [1.2 x 10^{24} atom-m^{-3} peak conc.] and Al (——) [6.7 x 10^{27} atom-m^{-3} peak conc.]; (b) uncorrected profile of ^{9}Be$^+$ (---) and ^{75}As$^+$ (——); (c) corrected profiles of Be (---) [2 x 10^{24} atom-m^{-3} full scale] and Al (——) [1 x 10^{28} atom-m^{-3} full scale] obtained assuming a linear concentration gradient at the interface; (d) corrected profiles of Be (---) [2 x 10^{24} atom-m^{-3} full scale] and Al (——) [1 x 10^{28} atom-m^{-3} full scale] obtained using the program SLIC (ref. 41).

homogeneous group IIIA - VA compound matrix can be quantified using the calibration lines and a single standard prepared from any of the group IIIA - VA compound matrices. There is no need to make a separate standard for each matrix. As shown earlier for Al$_x$Ga$_{1-x}$As matrices, these calibration lines also make the quantitative SIMS analysis of layered multimatrix samples possible. When the criteria necessary for SLIC are satisfied (for a homologous series of compounds such as Al$_x$Ga$_{1-x}$As, GaAs$_x$P$_{1-x}$ and InAs$_x$ Sb$_{1-x}$ where there is a common element of known concentration), very complex layered multimatrix samples may be quantitatively analyzed. When SLIC is not applicable, simpler structures with just a few well defined interfaces may be quantitatively analyzed by treating the interfaces as linear concentration gradients from one matrix (of predetermined composition) to another (the matrix-by-matrix approach). Both approaches have been applied to the hypothetical MBE structure illustrated in Fig. 9a. A ^{9}Be$^+$ concentration plateau approximately 0.1 μm wide and 1-2 x 10^{24} atom-m^{-3} high was grown by MBE while the matrix was linearly changed from GaAs to Al$_{.30}$Ga$_{.70}$As. In the uncorrected profile, Fig. 9b, the ^{9}Be distribution (dashed line) resembles a sharp spike rather than a plateau. In addition, the thickness and maximum concentration of the plateau can not be determined. The matrix corrected depth profiles using the matrix-by-matrix approach and SLIC are presented in Fig. 9c and 9d, respectively. The shape of the plateau differs slightly between the two versions of the corrected profile. However, both types of corrections allow a dramatic improvement over the uncorrected profile in the determination of plateau thickness and maximum concentration.

7. FUTURE TRENDS

These initial investigations into the calibration of the SIMS matrix effects for the quantitative analysis of multilayers of IIIA - VA semiconductors have established the ground work for future investigations. In particular, five important points have been made. First of all, both ion yields and sputtering yields were shown to vary linearly with the matrix composition of Al$_x$Ga$_{1-x}$As and similar series of IIIA - VA semiconductors. Second, matrix calibration lines were

shown to have superior precision and reproducibility when relative ion yields and relative sputtering yields are used instead of useful ion yields, relative sensitivity factor's, and sputtering yields. Third, a procedure for the quantitative SIMS analysis of multilayer-multimatrix samples has been established and incorporated into the program SLIC. Fourth, the investigation into the factors influencing matrix effects in group IIIA - VA semiconductors revealed that relative ion yield variations with matrix are a linear function of the matrix composition, and are influenced primarily by the oxygen affinity of the matrix constituents. Fifth, for elements in the same column of the periodic table, the influence of matrix effects on relative ion yields was shown to increase as the first ionization potential of the analyte increases.

While these accomplishments represent a significant advance in the development of quantitative SIMS analysis, matrix effect calibration, and depth profile correction, the mechanisms of matrix effects should all be examined in much greater detail. Due to the large inconsistency in the ion and sputtering yields obtained by any given laboratory, these parameters cannot critically be evaluated in the open literature. As a result, progress in the understanding of the sputtering and ion emission processes has been extremely slow. This difficulty could be minimized through the use of the more reproducible relative ion yield and sputtering yield values. Thus, it should be common practice to report R_T and RS values for all materials being examined by SIMS. In doing this, a single material (perhaps silicon) should be established internationally as the standard matrix for normalization. In this way, ion yields and sputtering yields obtained by different laboratories could be more readily compared and correlated. In particular, the R_T's and RS's of homologous matrices, such as metal silicides and germanides, should be examined for linear relationships like those established for the IIIA-VA semiconductors.

Any procedure for quantifying SIMS depth profiles through multimatrix films must consists of three steps: matrix identification, sputtering rate determination, and ion yield calibration. While SLIC is able to perform each of these steps simultaneously, the procedure used in SLIC to determine the matrix composition requires the presence of a single element (such as As in $Al_xGa_{1-x}As$) of known concentration in each of the layers. This requirement is not generally satisfied. Thus, a general method of matrix determination through layers is required to compliment the matrix effect calibration. One possible solution is the use of a second analytical technique (such as RBS or AES) to determine matrix composition and structure while matrix calibrated SIMS is used to determine the dopant distributions. As mentioned above, small mismatches in the matrix and trace element depth distributions can result in large errors in the matrix corrected trace element distributions. Thus, the critical factor in such a duel analysis approach is a coherent depth distribution match between the two data sets. Methods of insuring an adequate registration between the two data sets need to be developed.

The reproducible nature of R_T's should be exploited to determine mechanisms for the influence of matrix effects on useful ion yields. The data indicates that τ's are a function of matrix composition, and also the surface concentration of reactive primary species (oxygen and cesium). The surface concentration of reactive species depends on the availability of these species through surface adsorption and implantation during ion bombardment, and also on the oxygen affinity of the matrix. However, little work has been done to determine the relative importance of these factors and how experimental parameters may be altered to allow matrix calibration for a wider variety of samples. The contribution of adsorption, implantation, and matrix composition must be deconvoluted so that matrix effects observed for a variety of samples and analysis conditions may be understood.

REFERENCES

1. H. E. Beske, *Z. Naturforch.*, **22**, 459 (1959).

2. Z. Jurela, in "Atomic Collision Parameters in Solids," eds., D. W. Palmer, M. W. Thompson and P. D. Townsend, North-Holland, Amsterdam, p. 34, (1970).

3. G. M. McCracken, *Rep. Prog.*, *Phys.* **38**, 241 (1975).

4. G. Blaise and M. Bernheim, *Surf. Sci.* **47**, 324 (1975).

5. C. A. Andersen, *Int. J. Mass Spectrom. Ion Phys.* **3**, 413 (1970).

6. H. A. Storms, K. F. Brown and J. D. Stein, *Anal. Chem.* **49**, 2023 (1977)

7. K. Wittmaack, Rad. Eff. 63, 205 (1982).

8. S. Hofman, Appl. Phys. 13, 205 (1977).

9. P. H. Holloway and R. S. Bhattacharya, Surf. Interface Anal. 3, 118 (1981).

10. H. H. Anderson, in "Physics of Ionized Gases," ed., V. Vujnovic, Institute of
    Physics, Zagreb, p. 361 (1974).

11. Z. L. Liau, J. E. Lewis, H. S. Wildman and J. K. Howard, K. Surf. Sci., 1976,
    57, 393.

12. C. A. Anderson and J. R. Hinthorne, Anal. Chem., 45, 142 (1973).

13. A. E. Morgan and H. W. Werner, Anal. Chem. 48, 699 (1976).

14. Z. Jurela, Int. J. Mass Spectrom. Ion Phys. 37, 67 (1981).

15. Z. Sroubek, Surf. Sci., 44, 47 (1974).

16. J. M. Schroeer, T. N. Rhodin and R. C. Bradley, R. C. Surf. Sci. 34, 571
    (1973).

17. W. H. Gries, and W. L. Rauternbach, W. L. 6th Int. Symp. Microtechniques,
    Graz, Austria (1970).

18. W. H. Gries and E. Norval, Anal. Chim., Acta 75, 289 (1975).

19. D. P. Leta and G. H. Morrison, Anal. Chem. 52, 277 (1980).

20. D. P. Leta and G. H. Morrison, Anal. Chem. 52, 514 (1980).

21. V. R. Deline, C. A. Evans and P. Williams, Appl. Phys. Lett. 33, 578 (1978).

22. V. R. Deline, C. A. Evans W. Katz and P. William, Appl. Phys. Lett. 33, 832 (1978).

23. J. E. Chelgren, W. Katz, V. R. Deline, C. A. Evans, R. J. Blattner and
    P. Williams, J. Vac. Sci. Technol., 16, 324 (1979).

24. F. Schultz and K. Wittmaack, K. Rad. Eff. 29, 31 (1976).

25. H. Liebl., J. Vac. Sci. Technol. 12, 385 (1975).

26. P. V. Chu, Doctoral Thesis, Cornell University (1983).

27. K. Wittmaack, J. Appl. Phys. 52, 527 (1981).

28. K. Wittmaack, Appl. Surf., Sci. 9, 315 (1981).

29. A. E. Morgan, H. A. M. Grefte and H. J. Tolle, J. Vac. Sci. Technol. 18, 164 (1981).

30. C. Meyer, M. Maier and D. Bimberg, J. Appl. Phys. 54, 2627 (1983).

31. J. C. Pivin, C. Roques-Carmes and G. Slodzian, Int. J. Appl. Phys. 51, 4158 (1980).

32. J. C. Pivin, C. Roques-Carmes and G. Slodzian, J. Appl. Phys. 51, 4158 (1980).

33. A. Havette and G. Slodzian, J. Microsc. Spectrosc. Electron. 5, 131 (1980).

34. M. Yu and W. Reuter, J. Appl. Phys. 52, 1478 (1981).

35. M. Yu, J. Appl. Phys. 52, 1489 (1981).

36. K. Wittmaack, Surf. Sci. 112, 168 (1981).

37. W. Katz, Doctoral Thesis, University of Illinois (1978).

38. A. A. Galuska and G. H. Morrison, Anal. Chem. 55, 2051 (1983).

39. A. A. Galuska and G. H. Morrison, Anal. Chem. 56, 74 (1984).

40. J. W. Mayer, J. F. Ziegler, L. L. Chang, T. Tsu and L. Esaki, J. Appl. Phys.
    44, 2322 (1973).

41. A. A. Galuska and G. H. Morrison, Int. J. Mass Spectrum. Ion Processes, 61,
    59 (1984).